Chemical Science

ROYAL SOCIETY OF CHEMISTRY

EDGE ARTICLE

View Article Online
View Journal | View Issue

Cite this: *Chem. Sci.*, 2020, **11**, 11307

All publication charges for this article have been paid for by the Royal Society of Chemistry

Received 19th June 2020
Accepted 16th September 2020

DOI: 10.1039/d0sc03409f

rsc.li/chemical-science

Controlling cyclization pathways in palladium(II)-catalyzed intramolecular alkene hydrofunctionalization *via* substrate directivity†

Xin Wang,‡[ab] Zi-Qi Li,‡[a] Binh Khanh Mai,‡[c] John A. Gurak, Jr,[a] Jessica E. Xu,[a] Van T. Tran,[a] Hui-Qi Ni,[a] Zhen Liu,[a] Zhonglin Liu,[a] Kin S. Yang,[a] Rong Xiang,[b] Peng Liu *[c] and Keary M. Engle *[a]

We report a series of palladium(II)-catalyzed, intramolecular alkene hydrofunctionalization reactions with carbon, nitrogen, and oxygen nucleophiles to form five- and six-membered carbo- and heterocycles. In these reactions, the presence of a proximal bidentate directing group controls the cyclization pathway, dictating the ring size that is generated, even in cases that are disfavored based on Baldwin's rules and in cases where there is an inherent preference for an alternative pathway. DFT studies shed light on the origins of pathway selectivity in these processes.

Introduction

Catalytic alkene hydrofunctionalization reactions are of growing importance within the modern synthetic repertoire.[1] Among established methods for alkene hydrofunctionalization, palladium(II) catalysis involving Wacker-type nucleopalladation[2] followed by protodepalladation[3] of the resulting alkylpalladium(II) intermediate is an attractive approach because such reactions proceed in a redox-neutral manner and with ideal atom-economy.[4–7] Early intermolecular versions of such reactions were restricted to conjugated alkenes, such as enones and acrylates.[4] Pioneering work by Widenhoefer and Michael in the 2000s then established that non-conjugated alkenes could engage in palladium(II)-catalyzed intramolecular hydroalkylation (6-*endo-trig*)[5] and hydroamination (5/6-*exo-trig*)[6] with tethered 1,3-dicarbonyl and amide/carbamate nucleophiles, respectively (Scheme 1A). Building on these important precedents, our lab developed a substrate-directed approach to intermolecular hydrofunctionalization of non-conjugated alkenes with N–H and C–H (pro)nucleophiles that is highly regioselective, even with challenging 1,2-disubstituted alkene substrates (Scheme 1B).[7–9]

Results and discussion

Based on these precedents, we questioned whether it would be possible to control the regioselectivity of intramolecular hydrofunctionalization through substrate directivity,[10,11] whereby the directing group would override any inherent pathway bias and enhance reactivity with more highly substituted alkenes (Scheme 1C). In this way, we envisioned that this approach could grant access to product structures that are not readily accessible using existing hydrofunctionalization methods, thereby complementing other approaches. At the outset, we anticipated several potential challenges that would need to be overcome to reduce this idea to practice, including the attenuated reactivity of more substituted nucleophiles (*e.g.*, protected alkyl amine compounds), the diminished reactivity of internal alkenes, and the fact that inherent ring-closing tendencies may compete (or even predominate) against the directed pathway. Additionally, our previous attempts to integrate oxygen-based nucleophiles in directed intermolecular nucleopalladation systems had been unsuccessful, presumably due to the endergonic and reversible nature of C–O bond formation.[12]

To initiate our investigation, we elected to use alkenyl amine **1c** as our pilot substrate, which we hypothesized would react *via* 6-*exo-trig* cyclization facilitated by the 8-aminoquinoline-derived amide directing group (AQ) (Table 1). Using $Pd(OAc)_2$ as precatalyst and MeCN as solvent, we evaluated a series of carboxylic acid additives (entries 1–6) and found that sterically bulky aliphatic acids led to slightly better yields, with 1-$AdaCO_2H$ being the best among those tested (entry 1). Another key finding was that polar aprotic solvents, such as MeCN and PhCN, outperformed nonpolar solvents, and that acidic protic solvents, such as HFIP and TFE, led to diminished yields

[a]*Department of Chemistry, The Scripps Research Institute, 10550 North Torrey Pines Road, La Jolla, California 92037, USA. E-mail: keary@scripps.edu*

[b]*Department of Medicinal Chemistry, School of Medicine, Nankai University, 94 Weijin Road, Tianjin 300071, China*

[c]*Department of Chemistry, University of Pittsburg, Pittsburgh, Pennsylvania 15260, USA. E-mail: pengliu@pitt.edu*

† Electronic supplementary information (ESI) available. CCDC 1995204. For ESI and crystallographic data in CIF or other electronic format see DOI: 10.1039/d0sc03409f

‡ These authors contributed equally to this work.

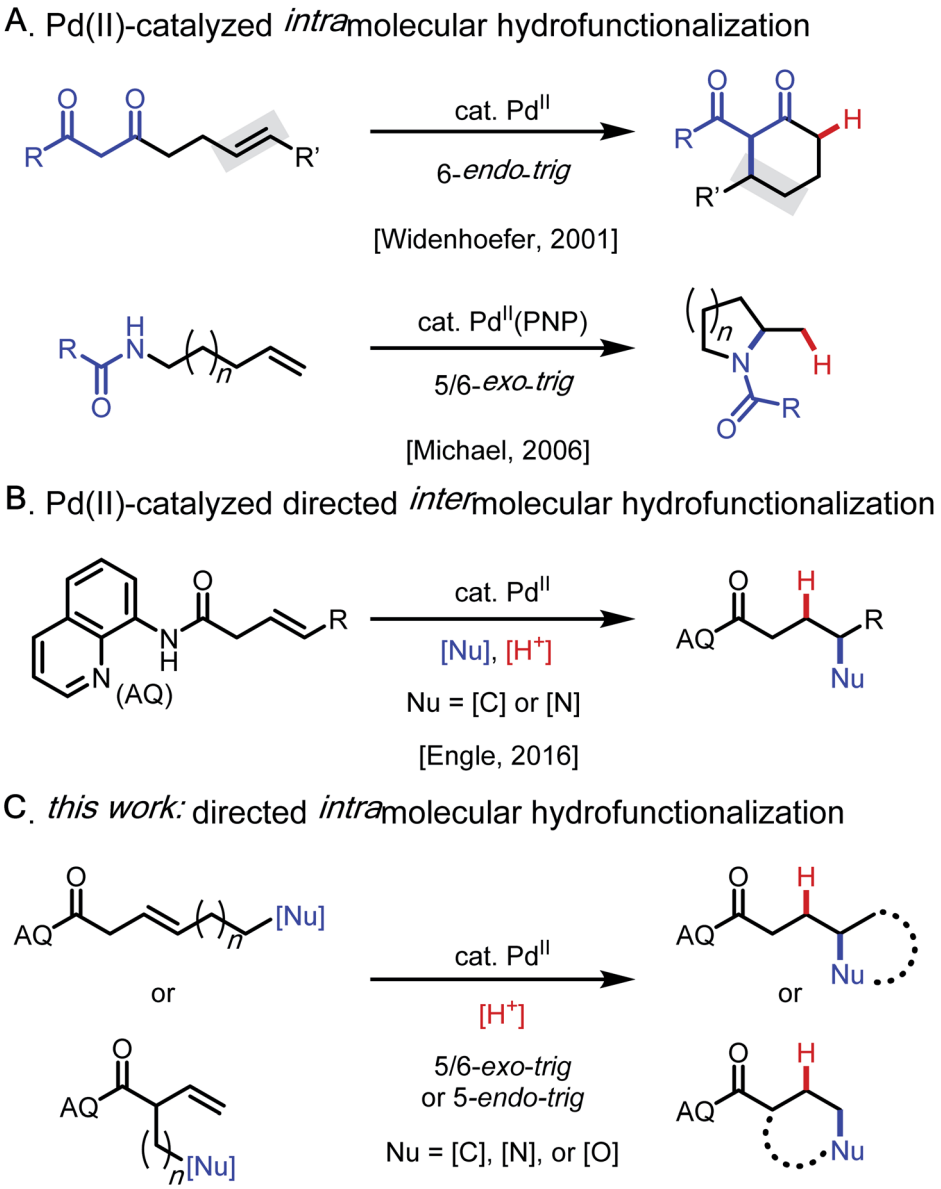

Scheme 1 Background and synopsis of current work.

(entries 7–11). When the reaction temperature was reduced to 80 °C, slightly lower yield was observed, even when the reaction time was extended (entry 12). Raising the temperature to 120 °C led to partial decomposition of the substrate, with a concomitant reduction in yield (78% yield, entry 13). Interestingly, unlike many other intramolecular cyclization reactions, this reaction gives high yields at higher concentration (entries 14 and 15). This suggests that intermolecular oligomerization is not a competitive process. Directing groups that are similar in structure to AQ but less rigid (**DG1** and **DG2**) only gave 44% and 16% yield, respectively (entries 16 and 17). The corresponding free carboxylic acid substrate decomposed under the reaction condition, and in this case, the desired product could not be detected. These results illustrate the importance of the AQ group for promoting the desired reaction pathway.

After identifying optimal reaction conditions, we turned our attention to examining the scope and limitations of this protocol. First, ring size effects were tested with substrates bearing different chain length. Based on Baldwin's rules, 4-, 5-, 6- and 7-*exo-trig* ring closure are all predicted to be allowed.[13,14] However, only product **2ba** and **2ca**, corresponding to the 5-*exo-trig* and 6-*exo-trig* pathways, respectively, were formed in high yields. In the other two cases, only unreacted starting material could be recovered. Based on the results above, we next investigated the N-substituent compatibility of the reaction. For the 5-*exo-trig* cyclization, changing the R group to Cbz, Ms, or Ts gave similar yields of around 90% (**2bb–2bd**), while a more electron-withdrawing group (Ns) only gave 73% yield (**2be**). Similar trends were observed with the 6-*exo-trig* pathway, where the Ns-protected substrate furnished only 32% yield (**2ce**). Other sulfonamide substituents provided good to excellent yield (**2cf–**

Table 1 Optimization of reaction conditions for intramolecular hydroamination of **1c**[a]

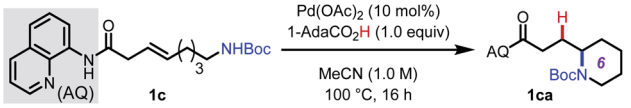

Entry[a]	Variation from standard conditions	Yield[b]
1	**(None)**	**97% (92%)**
2	AcOH in place of 1-AdaCO$_2$H	89%
3	PivOH in place of 1-AdaCO$_2$H	92%
4	PhCO$_2$H in place of 1-AdaCO$_2$H	87%
5	**A1** in place of 1-AdaCO$_2$H	90%
6	**A2** in place of 1-AdaCO$_2$H	88%
7	PhMe as solvent	82%
8	PhCN as solvent	88%
9	*t*-AmylOH as solvent	77%
10	TFE as solvent	77%
11	HFIP as solvent	65%
12[c]	80 °C	91%
13	120 °C	78%
14	0.5 M	96%
15	2.0 M	90%
16[d]	**DG1** in place of AQ	44%
17[d]	**DG2** in place of AQ	16%
18[d]	OH in place of AQ	n.d.

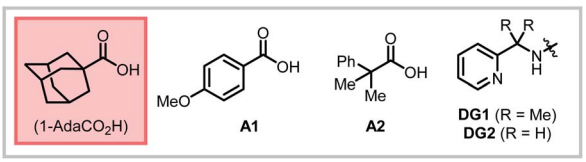

[a] **1c** (0.1 mmol). [b] ^{1}H NMR yield with CH_2Br_2 as internal standard; isolated yield given in parentheses. [c] 40 h. [d] **1c** (0.05 mmol).

Table 2 Electrophile and nucleophile scope[a]

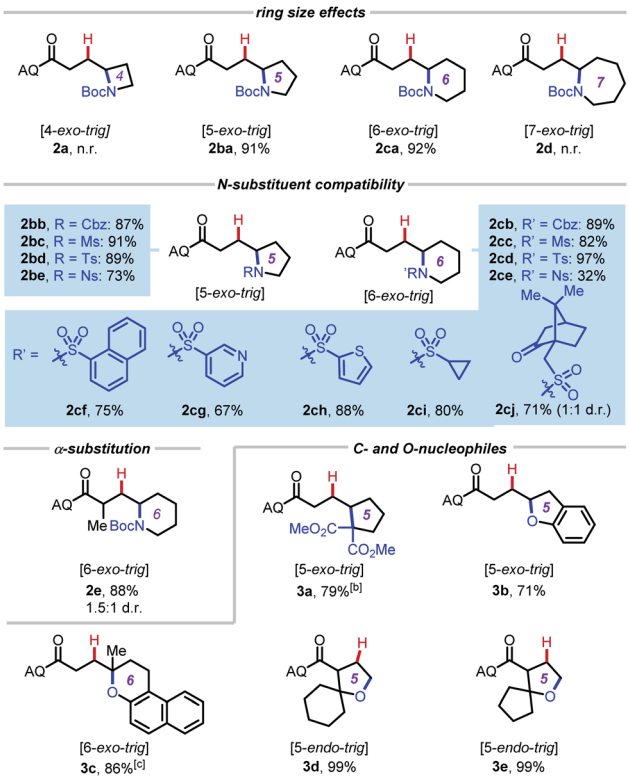

[a] Reactions performed on 0.1 mmol scale using standard conditions from Table 1 unless otherwise specified. Percentages represent isolated yields. [b] HFIP was used as solvent. [c] Reaction was performed on 0.012 mmol scale and at 0.5 M concentration. The reduced scale in this case reflects difficulties in preparing pure starting material (see ESI).

2cj). Gratifyingly, heterocyclic substituents were competent, with 3-pyridyl (**2cg**) and 2-thiofuranyl sulfonamides (**2ch**) giving 67% and 88% yields, respectively. We examined the effect of substitution at the α-position and found that 6-*exo-trig* cyclization with a Boc-protected nitrogen nucleophile proceeded in 88% yield and 1.5 : 1 d.r. (**2e**).

We next questioned whether directed cyclization was possible with carbon- and oxygen-based nucleophiles. Not only could this expand the utility of this approach, but it would also allow us to test whether substrate directivity could enforce otherwise disfavored ring closures across diverse substrate classes. To this end, we tested a series of substrates bearing potentially reactive nucleophiles at various positions. Indeed, we found that a substrate bearing tethered malonate nucleophile, reacted in a 5-*exo-trig* mode, rather than the 6-*endo-trig* mode documented by Widenhoefer,[5] to give the product **3a** in 79% yield with HFIP as the optimal solvent. This example underscores the complementary nature of directed and non-directed metal-catalyzed cyclizations. Though oxygen-based nucleophiles have not been extensively studied in palladium(II)-catalyzed hydrofunctionalization reactions with non-conjugated alkenes, we were pleased to find that alkenyl alcohols were competent substrates under these conditions. A tethered phenol nucleophile reacted in a 5-*exo-trig* mode to give product **3b** in 71% yield. Likewise, with a tethered naphthol nucleophile, 6-*exo-trig* cyclization onto a trisubstituted alkene proceeded in 86% yield (**3c**). We have previously shown that product **3c** can alternatively be prepared by a cascade process from 2-naphthol and the corresponding 1,3-diene, where this trisubstituted alkenyl alcohol is generated *in situ* (see ESI†).[10] Additionally, we found that oxaspiro compounds **3d** and **3e** could be synthesized in nearly quantitative yields through a mechanism involving a Baldwin's-disallowed 5-*endo-trig* cyclization.[15]

To interrogate the mechanistic underpinnings and origins of regioselectivity in these reactions, we next performed a series of mechanistic experiments. We first prepared π-alkene palladium complex **4** by combining $Pd(OAc)_2$ (1 equiv.) with a representative alkenyl amine derivative and characterized it by NMR and X-ray crystallography. In the X-ray structure, the substrate binds analogously to related examples with alkenyl AQ-amide substrates;[7a,7b] however in this case the pendant nucleophile occupies the fourth coordination site as an X-type ligand, such that the substrate adopts an overall tetradentate coordination mode. We next probed for the possibility of *E*/*Z* isomerization[16] during the course of catalysis, which is important in

establishing what cyclization pathways are potentially operative in the reaction. To this end, we subjected substrate **1c** to the reaction conditions, and halted the reaction prematurely. In this case, we were able to observe a mixture of product **2ca**, small amounts of other alkene isomers, and recovered starting material **1c** (*E*/*Z* ratio = 8 : 1). The presence of *Z*-isomer, albeit in small amounts, establishes that reaction through either isomer is potentially possible in this system,[16b,16c] which complicates experimental interrogation of the mechanism.

A general mechanism of this palladium-catalyzed intramolecular hydrofunctionalization process is shown in Scheme 3.[7] $Pd(OAc)_2$ coordinates to the aminoquinoline directing group and the alkene moiety on the substrate to form a π-alkene complex, which then undergoes nucleopalladation, protodepalladation, and ligand exchange to generate the hydroamination product. Several pertinent mechanistic questions remained outstanding: (1) What is the mechanism of nucleopalladation? (2) How does tether length affect the reactivity? (3) Which factors control the regioselectivity of the hydroamination? To seek a better understanding of these questions, we turned our efforts to density functional theory (DFT) calculations.[17]

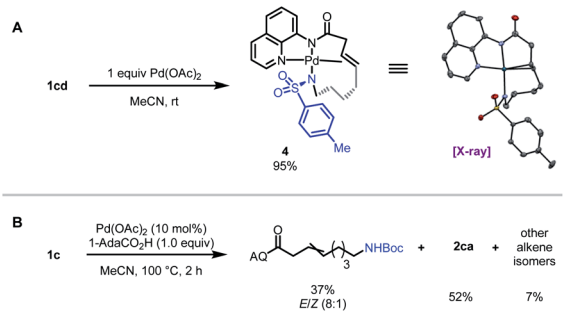

Scheme 2 Mechanistic experiments.

The computational studies were initiated by elucidating the reaction mechanisms of the intramolecular cyclization of alkenyl amine **1b**, which forms the 5-*exo-trig* product **2ba** with high regioselectivity (Table 2).[18] Several potential *syn*- and *anti*-nucleopalladation processes to access the 5-*exo-trig* and 6-*endo-trig* cyclization products were considered. The most favorable pathway, as shown in Fig. 1, involves tetradentate square-planar complex **IM2b** formed *via* the acetate-assisted concerted metalation/N–H deprotonation *via* **TS1b**. In **IM2b**, the pendent nucleophile occupies the coordination site *cis* to the alkene, a geometry akin to the X-ray crystal structure of **4** (Scheme 2). From **IM2b**, intramolecular *syn*-nucleopalladation takes place *via* **TS2b**. This 5-*exo-trig* cyclization process leads to palladacycle intermediate **IM3b**, which then undergoes protodepalladation *via* **TS3b** to form product complex **IM4b**. The β-hydride elimination (**TS4b**) requires a 2.2 kcal mol^{-1} higher barrier than that of protodepalladation and forms a thermodynamically less stable palladium–hydride complex **IM6b**. These results agree with the absence of β-hydride elimination products in the crude reaction mixture. Finally, ligand exchange with another reactant molecule releases the hydroamination product **2ba** and regenerates the π-alkene complex **IM1b**. The computed activation free energies of several less favorable nucleopalladation pathways are summarized in Table 3 (entry 2). Transition state **TS5b** involves *syn*-nucleopalladation from the π-alkene complex **IM1b**. Here, the deprotonation of the Boc-protected amine and the nucleopalladation take place in a concerted fashion. Although **TS5b** is slightly less stable by 2.1 kcal mol^{-1}, the relatively small energy difference between **TS2b** and **TS5b** suggests that both processes may be operative depending on the substrate (*vide infra*). *anti*-Nucleopalladation pathways to access

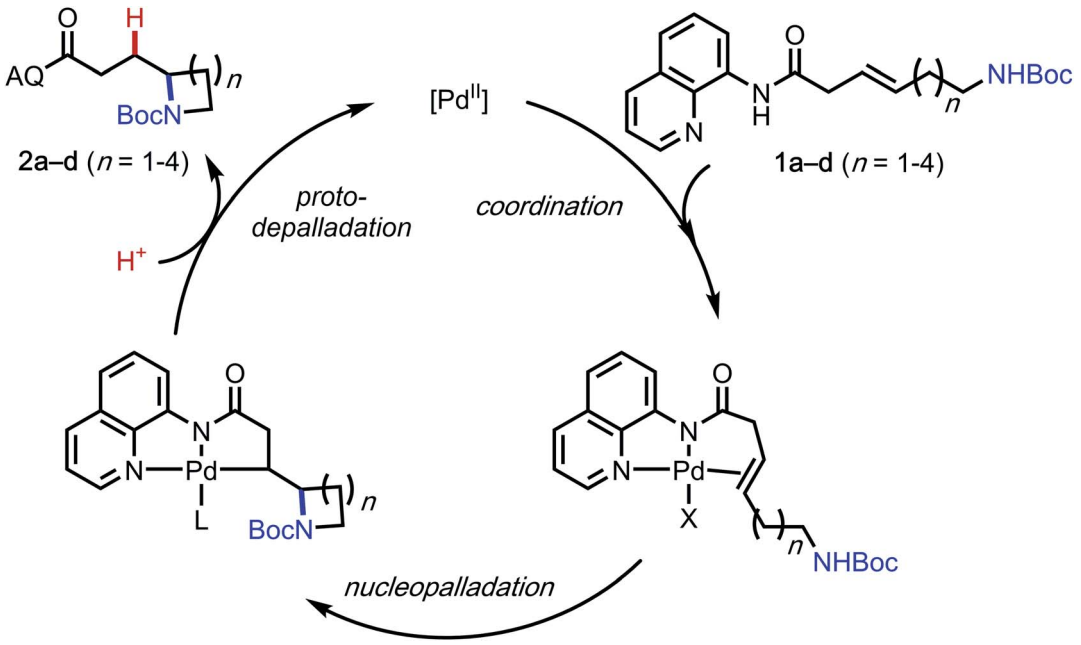

Scheme 3 General depiction of a plausible reaction mechanism.

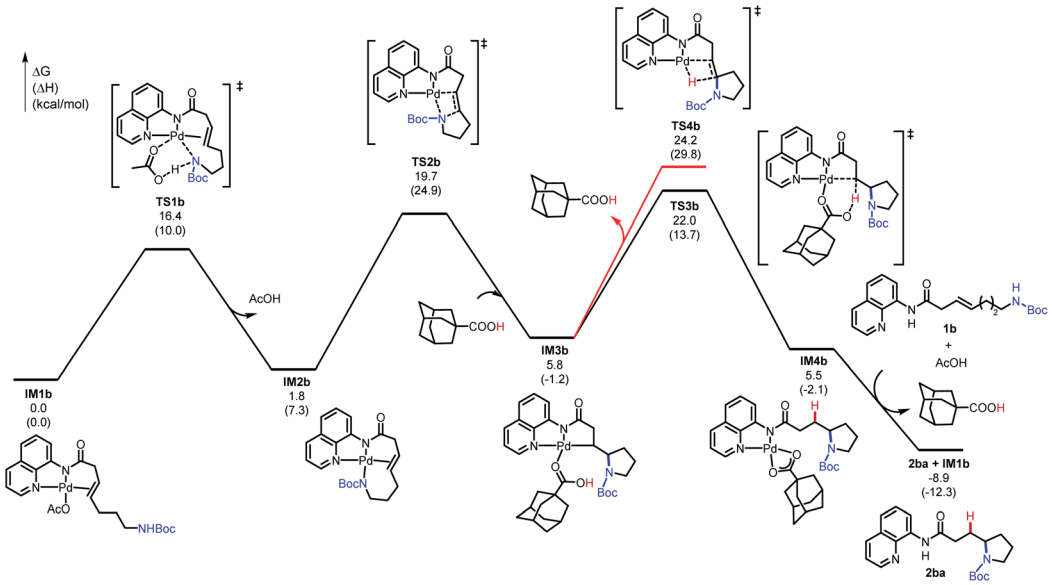

Fig. 1 Computed energy profile of the 5-*exo*-*trig* cyclization of **1b** (see ESI† for energy profiles of 4-, 6-, and 7-*exo*-*trig* cyclizations of **1a**, **1c**, and **1d**).

the 5-*exo*-*trig* and 6-*endo*-*trig* cyclization products (**TS6b** and **TS7b**) are both much less favorable than **TS2b**. Furthermore, the *syn*-nucleopalladation transition state leading to the 6-*endo*-*trig* product is highly distorted and is 13.7 kcal mol^{-1} less favorable than **TS2b** (see Fig. S8†). Here, *syn*-nucleopalladation pathways for 5-*exo*-*trig* cyclization (**TS2b** and **TS5b**) are the most favorable due to either facile deprotonation of the Boc-protected amine to form **IM2b** or a concerted N–H deprotonation during nucleopalladation. Both scenarios provide stronger nucleophiles relative to the protonated state, which facilitate the ring formation. By contrast, N–H deprotonation in *anti*-nucleopalladation pathways is disfavored due to the low acidity of the (alkyl)NHBoc group.[19] The less nucleophilic protonated state is involved in the *anti*-nucleopalladation, leading to their higher activation energies. Because the *anti*-nucleopalladation pathways are less regioselective (*i.e.* the activation energies of **TS6b** and **TS7b** are comparable), the lower activation energy of *syn*-nucleopalladation in 5-*exo*-*trig* cyclization plays an important role in controlling the regioselectivity of the cyclization product.

We then evaluated the effects of ring size on the mechanisms of nucleopalladation. Computed activation barriers of (n + 3)-*exo*-*trig* and (n + 4)-*endo*-*trig* pathways (n = 1–4) of alkenyl amines **1a–d** are summarized in Table 3. The most favorable cyclization mechanism depends upon the ring-size. Computationally, reaction with **1a** favors the 5-*endo*-*trig* cyclization due to the high ring-strain of the four-membered azetidine ring[20] in the 4-*exo*-*trig* pathway (entry 1), but experimentally neither putative products are observed. In reactions with **1b–d**, the *syn*-nucleopalladation leading to the 5-, 6-, and 7-*exo*-*trig* products are always favored, with either the N–H-deprotonated amide or the neutral Boc-protected amine as the active nucleophile (**TS2** and **TS5**, respectively). Although both 6- and 7-*endo*-*trig* ring closures are allowed based on Baldwin's rules, these pathways with **1b** and **1c** require 4.9 and 10.5 kcal mol^{-1} higher barriers than corresponding 5- and 6-*exo*-*trig* pathways to form **2ba** and **2ca**.

Ring size also plays a significant role in the activation barriers of the nucleopalladation. *syn*-Nucleopalladation with **1a** and **1d** *via* 4- and 7-*exo*-*trig* cyclization require much higher barriers (29.3 and 27.1 kcal mol^{-1}, respectively) than the 5- and 6-*exo*-*trig* cyclizations with **1b** and **1c** (19.7 and 21.7 kcal mol^{-1}, respectively). This trend agrees with the fact that four- and seven-membered ring products were not observed in experiments. It should be noted that the reactivity trend in cyclization does not completely follow the trend of the strain energies[20] of the heterocycle products (Fig. 2). For example, although the strain energies of pyrrolidine (n = 2) and azepane (n = 4) are comparable, the cyclization to form the latter requires a substantially higher activation energy. In addition, formation of the less-strained piperidine (n = 3) requires a higher energy barrier than that of pyrrolidine (n = 2). Our results suggest that besides the ring strain of the cyclization product, steric effects also contribute to the activation energies of *syn*-nucleopalladation. Greater steric repulsions between the nitrogen nucleophile and the AQ directing group are observed in the *syn*-nucleopalladation transition states to form larger rings (*e.g.* seven-membered. See **TS2d** in Fig. 3).

Next, we evaluated the barriers of protodepalladation to investigate whether nucleopalladation or protodepalladation is rate- and selectivity-determining. The stabilities of palladacycle **IM3** and the subsequent protodepalladation transition state (**TS3**) both have good correlation with the ring strain energy of the formed N-heterocycle (see ESI† for details).[20b] This indicates steric effects of the N-heterocycle play a less important role in the protodepalladation step. In reactions with **1a–1c**, the protodepalladation requires a higher barrier than the nucleopalladation, and is thus rate-determining.[21] While with **1d**,

Table 3 Gibbs free energies of stationary points in the Pd-catalyzed intramolecular hydroamination of **1a–d**. All energy values (in kcal mol^{-1}) are relative to **IM1**. Bold numbers indicate the most favorable mechanisms in the nucleopalladation step

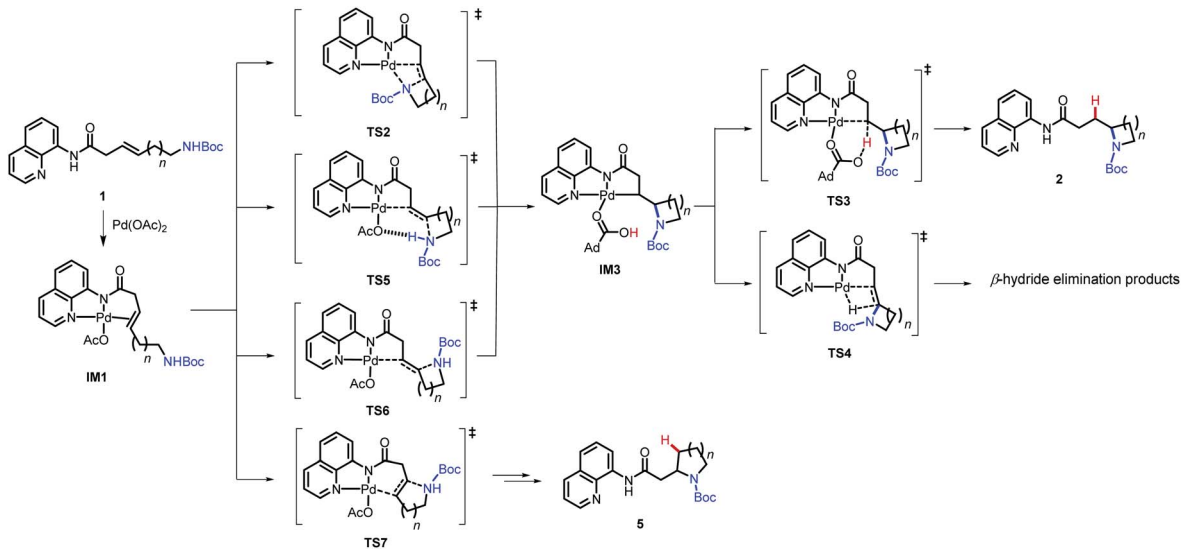

		(*n* + 3)-*Exo-trig*			(*n* + 4)-*Endo-trig*	(*n* + 3)-*Exo-trig*		
		syn-Nucleo-palladation TS		*anti*-Nucleo-palladation TS	*anti*-Nucleo-palladation TS	Pallada-cycle	Protode-palladation TS	β-Hydride elimination TS
Entry	Alkenyl amine	**TS2**	**TS5**	**TS6**	**TS7**	**IM3**	**TS3**	**TS4**
1	**1a** ($n = 1$)	31.0	29.3	Cannot locate	**28.0**	21.8[a]	39.6[a]	37.6
2	**1b** ($n = 2$)	**19.7**	21.8	24.0	24.6	5.8	22.0	24.2
3	**1c** ($n = 3$)	23.3	**21.7**	24.9	32.2	5.7	22.7	23.9
4	**1d** ($n = 4$)	**27.1**	29.1	31.3	Cannot locate	8.1	24.5	26.9

[a] In the reaction with **1a**, the 5-*endo-trig* regioisomeric pathway is more favorable. The Gibbs free energies of the palladacycle and the protodepalladation TS in the 5-*endo-trig* pathway with **1a** are 9.2 and 29.4 kcal mol^{-1}, respectively.

nucleopalladation was calculated to be the highest-energy step due to the unfavorable steric repulsions in **TS2d**.

Furthermore, we computed the reaction energy profile of the Baldwin-disallowed 5-*endo-trig* cyclization giving oxaspiro compound **3d** (see Fig. S6 in the ESI†). The cyclization occurs *via* an *anti*-nucleopalladation TS that only requires 26.0 kcal mol^{-1} relative to the π-alkene complex. The *syn*-nucleopalladation TS with this substrate is less favorable due to steric repulsions between the spiro center and the Pd. The relatively low barrier in the *anti*-nucleopalladation is in accordance with the effective formation of 5-*endo-trig* cyclization products experimentally. One likely contributor for preference for this mode of closure, in this case, is the fact that 4-*exo-trig* cyclization is disfavored

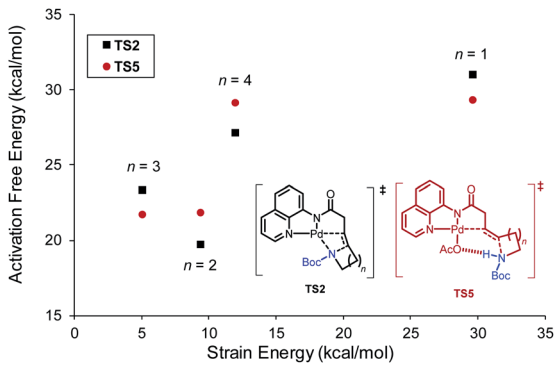

Fig. 2 Activation free energies of *syn*-nucleopalladation transition states relative to **IM1** and strain energies of the N-heterocycles.[20b]

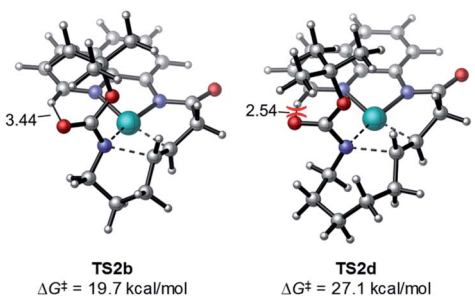

Fig. 3 Greater steric repulsions in the *syn*-nucleopalladation transition state **TS2d** to form a seven-membered ring.

because of the high ring-strain of the four-membered oxetane ring.[20]

Conclusions

In conclusion, we developed a palladium catalyzed intramolecular hydrofunctionalization system with 8-aminoquinoline as directing group. This method can tolerate a variety of nucleophiles including nitrogen-, oxygen- and carbon-based nucleophiles. Moreover, a Baldwin's rule disallowed 5-*endo-trig* cyclization was achieved for the preparation of a unique spirocycle. A detailed mechanistic study was performed. For the 5-*exo-trig* and 6-*exo-trig* cyclization, the reaction proceeds through a *syn*-addition, protodepalladation pathway. For the Baldwin's-disallowed 5-*endo-trig* cyclization, on the other hand, the computational results favor an *anti*-nucleopalladation pathway. Further studies on achieving the asymmetric version of this transformation are in progress in our lab.

Conflicts of interest

There are no conflicts to declare.

Acknowledgements

This work was financially supported by the NIH (R35GM125052-03, R35GM128779). We further acknowledge the China Scholarship Council for visiting student scholarship (X. W.), the NSF for a Graduate Research Fellowship (DGE-1346837, J. A. G.), the Life Science Summer Institute for an internship (J. E. X.), and Bristol-Myers Squibb for a Graduate Fellowship (Z. L.). We thank Prof. Arnold L. Rheingold (UCSD) for X-ray crystallographic analysis. DFT calculations were performed at the Center for Research Computing at the University of Pittsburgh and the Extreme Science and Engineering Discovery Environment (XSEDE) supported by the National Science Foundation grant number ACI-1548562. Zibo Bai and Prof. Gong Chen (Nankai University) are acknowledged for helpful discussion.

Notes and references

1 For representative reviews, see: (*a*) N. A. Foley, J. P. Lee, Z. Ke, T. B. Gunnoe and T. R. Cundari, *Acc. Chem. Res.*, 2009, **42**, 585–597; (*b*) L. Huang, M. Arndt, K. Gooßen, H. Heydt and L. J. Gooßen, *Chem. Rev.*, 2015, **115**, 2596–2697; (*c*) K. D. Hesp and M. Stradiotto, *ChemCatChem*, 2010, **2**, 1192–1207; (*d*) Y. Yamamoto and U. Radhakrishnan, *Chem. Soc. Rev.*, 1999, **28**, 199–207.

2 For reviews, see: (*a*) K. H. Jensen and M. S. Sigman, *Org. Biomol. Chem.*, 2008, **6**, 4083–4088; (*b*) R. I. McDonald, G. Liu and S. S. Stahl, *Chem. Rev.*, 2011, **111**, 2981–3019; (*c*) P. Kočovský and J.-E. Bäckvall, *Chem.–Eur. J.*, 2015, **21**, 36–56; (*d*) G. Yin, X. Mu and G. Liu, *Acc. Chem. Res.*, 2016, **49**, 2413–2423.

3 M. L. O'Duill and K. M. Engle, *Synthesis*, 2018, **50**, 4699–4714.

4 (*a*) M. A. Stark and C. J. Richards, *Tetrahedron Lett.*, 1997, **38**, 5881–5884; (*b*) M. A. Stark, G. Jones and C. J. Richards, *Organometallics*, 2000, **19**, 1282–1291; (*c*) M. J. Gaunt and J. B. Spencer, *Org. Lett.*, 2001, **3**, 25–28; (*d*) K. Takenaka and Y. Uozumi, *Org. Lett.*, 2004, **6**, 1833–1835. For related processes involving Heck-type migratory insertion, see: (*e*) K. Yamamura, *J. Org. Chem.*, 1978, **43**, 724–727; (*f*) S. Cacchi, F. La Torre and D. Misiti, *Tetrahedron Lett.*, 1979, **20**, 4591–4594; (*g*) X. Lu and S. Lin, *J. Org. Chem.*, 2005, **70**, 9651–9653.

5 (*a*) T. Pei and R. A. Widenhoefer, *J. Am. Chem. Soc.*, 2001, **123**, 11290–11291; (*b*) H. Qian and R. A. Widenhoefer, *J. Am. Chem. Soc.*, 2003, **125**, 2056–2057.

6 (*a*) F. E. Michael and B. M. Cochran, *J. Am. Chem. Soc.*, 2006, **128**, 4246–4247; (*b*) B. M. Cochran and F. E. Michael, *J. Am. Chem. Soc.*, 2008, **130**, 2786–2792.

7 (*a*) J. A. Gurak Jr, K. S. Yang, Z. Liu and K. M. Engle, *J. Am. Chem. Soc.*, 2016, **138**, 5805–5808; (*b*) K. S. Yang, J. A. Gurak Jr, Z. Liu and K. M. Engle, *J. Am. Chem. Soc.*, 2016, **138**, 14705–14712; (*c*) J. A. Gurak Jr, V. T. Tran, M. M. Sroda and K. M. Engle, *Tetrahedron*, 2017, **73**, 3636–3642.

8 We and others have shown that such processes can be rendered enantioselective in the presence of an appropriate chiral promoter: (*a*) H. Wang, Z. Bai, T. Jiao, Z. Deng, H. Tong, G. He, Q. Peng and G. Chen, *J. Am. Chem. Soc.*, 2018, **140**, 3542–3546; (*b*) H.-C. Shen, L. Zhang, S.-S. Chen, J. Feng, B.-W. Zhang, Y. Zhang, X. Zhang, Y.-D. Wu and L.-Z. Gong, *ACS Catal.*, 2019, **9**, 791–797; (*c*) S. K. Nimmagadda, M. Liu, M. K. Karunananda, D.-W. Gao, O. Apolinar, J. S. Chen, P. Liu and K. M. Engle, *Angew. Chem., Int. Ed.*, 2019, **58**, 3923–3927; (*d*) C. Wei, X. Ye, Q. Xing, Y. Hu, Y. Xie and X. Shi, *Org. Biomol. Chem.*, 2019, **17**, 6607–6611.

9 For related reactions involving Heck-type organopalladium migratory insertion followed by protodepalladation, see: (*a*) R. Matsuura, T. C. Jankins, D. E. Hill, K. S. Yang, G. M. Gallego, S. Yang, M. He, F. Wang, R. P. Marsters, I. McAlpine and K. M. Engle, *Chem. Sci.*, 2018, **9**, 8363–8368; (*b*) Z. Bai, Z. Bai, F. Song, H. Wang, G. Chen and G. He, *ACS Catal.*, 2020, **10**, 933–940.

10 In ref. 7*b* our lab described a cascade reaction of 1,3-dienes in which intramolecular alkene hydrofunctionalization was proposed as the second step. Prior to the present study, this cyclization process had not been studied systematically in isolation.

11 For a related 1,1-heterodifunctionalization process involving intramolecular trapping, see: J. Jeon, H. Ryu, C. Lee, D. Cho, M.-H. Baik and S. Hong, *J. Am. Chem. Soc.*, 2019, **141**, 10048–10059.

12 (*a*) V. T. Tran, J. A. Gurak Jr, K. S. Yang and K. M. Engle, *Nat. Chem.*, 2018, **10**, 1126–1133; (*b*) H.-Q. Ni, I. Kevlishvili, P. G. Bedekar, J. S. Barber, S. Yang, M. Tran-Dubé, H.-X. Lu, I. McAlpine, P. Liu and K. M. Engle, *ChemRxiv*, 2020, DOI: 10.26434/chemrxiv.12510038.

13 J. E. Baldwin, *J. Chem. Soc., Chem. Commun.*, 1976, 734–736.

14 It should be noted that transition-metal-mediated cyclizations are mechanistically distinct processes from those included in Baldwin's original empirical models and

thus exhibit distinct reactivity trends in some cases. For a computational analysis of intramolecular migratory insertion pathways, see: B. Fiser, J. M. Cuerva and E. Gómez-Bengoa, *Organometallics*, 2018, **37**, 390–395.

15 While this work was in progress, this O-cyclization method was used to prepare one starting material in ref. 12*a*.

16 (*a*) Z. Liu, T. Zeng, K. S. Yang and K. M. Engle, *J. Am. Chem. Soc.*, 2016, **138**, 15122–15125; (*b*) Z. Liu, X. Li, T. Zeng and K. M. Engle, *ACS Catal.*, 2019, **9**, 3260–3265; (*c*) Z. Bai, S. Zheng, Z. Bai, F. Song, H. Wang, Q. Peng, G. Chen and G. He, *ACS Catal.*, 2019, **9**, 6502–6509.

17 DFT calculations were performed at the M06/6-311+G(d,p)-SDD/SMD(MeCN)//M06/6-31G(d)-SDD level of theory. See the ESI† for computational details.

18 Because *E*/*Z* isomerization of the alkene was observed experimentally, we also calculated the cyclization of the *Z*-isomers of **1a–d**. The calculations indicate that the reactions with the *Z*-isomers are less favorable (see ESI†).

19 In the reaction with **1c**, the *anti*-nucleopalladation transition state with the deprotonated N-nucleophile is 2.9 kcal mol^{-1} higher in energy than **TS6c**. This transition state is disfavored due to the high energy required (21.1 kcal mol^{-1}) to deprotonate the (alkyl)NHBoc with OAc^- as the base. It should be noted that reactions with a more acidic nucleophile (*e.g.*, succinimide) may occur with the nucleophile in its deprotonated state and that this may be a contributing factor for the experimentally observed preference for *anti*-nucleopalladation in previously reported intermolecular systems (see ref. 7).

20 (*a*) S. W. Benson, F. R. Cruickshank, D. M. Golden, G. R. Haugen, H. E. O'Neal, A. S. Rodgers, R. Shaw and R. Walsh, *Chem. Rev.*, 1969, **69**, 279–324; (*b*) T. Dudev and C. Lim, *J. Am. Chem. Soc.*, 1998, **120**, 4450–4458.

21 Although protodepalladation is turnover-limiting in reactions with **1b** and **1c**, the regioselectivity in these reactions is still controlled in the nucleopalladation step, because the 6- and 7-*endo-trig* nucleopalladation transition states (**TS7b** and **TS7c**) have higher barriers than the protodepalladation transition states in the 5- and 6-*exo-trig* pathways (**TS3b** and **TS3c**).